Radiation Physics and Chemistry 79 (2010) 185–194

Contents lists available at ScienceDirect

Radiation Physics and Chemistry

journal homepage: www.elsevier.com/locate/radphyschem

Applications of X-ray absorption spectroscopy to biologically relevant metal-based chemistry

Stephen P. Best *, Mun Hon Cheah

School of Chemistry, University of Melbourne, Melbourne, Victoria 3010, Australia

ARTICLE INFO

Article history:
Received 15 November 2008
Accepted 15 March 2009

Keywords:
Hydrogenase
Nitrogenase
Metal carbonyls
Electrocatalysis
X-ray absorption spectroscopy
Nuclear resonance vibrational spectroscopy
Density functional theory
EXAFS

ABSTRACT

Recent developments in the understanding of the biosynthesis of the active site of the nitrogenase enzyme, the structure of the iron centre of [Fe]-hydrogenase and the structure and biomimetic chemistry of the [FeFe] hydrogenase H-cluster as deduced by application of X-ray spectroscopy are reviewed. The techniques central to this work include X-ray absorption spectroscopy either in the form of extended X-ray absorption fine structure (EXAFS), X-ray absorption near-edge structure (XANES) and nuclear resonant vibrational spectroscopy (NRVS). Examples of the advances in the understanding of the chemistry of the system through integration of a range of spectroscopic and computational techniques with X-ray spectroscopy are highlighted. The critical role played by *ab initio* calculation of structural and spectroscopic properties of transition-metal compounds using density functional theory (DFT) is illustrated both by the calculation of nuclear resonance vibrational spectroscopy (NRVS) spectra and the structures and spectra of intermediates through the catalytic reactions of hydrogenase model compounds.

1. Introduction

Metalloenzymes encapsulate the chemical machinery needed to crack the hardest problems in biology and industry; this is perhaps no better illustrated by the activation of simple, strongly bound molecules such as N_2 (Burgess and Lowe, 1996; Holland, 2004; Howard and Rees, 2006) and H_2 (Morris, 2006; Tolman, 2006; Vignais and Billoud, 2007). The evolutionary solution to problems of this sort has been to construct highly sophisticated polypeptide scaffolds to constrain the co-ordination environment of the transition-metal cofactors so as to tune the catalytic reactions (Bertini et al., 1994; Duhme-Klair, 2008; Hinnemann and Norskov, 2006; Spiro, 2007). Identification of the structure, the molecular details of the reaction path and even the composition of the cofactors represent significant challenges that both drive and benefit from advances in fundamental science. While this contribution concentrates on some recent examples involving the application of synchrotron X-radiation, it is important to emphasize that it is the combination of a range of experimental and computational methods that underpin the recent advances in understanding of the structure and operation of metalloenzymes. Focus on the nitrogenase and hydrogenase enzymes is driven in equal measure by the drive to establish a coherent, evidence-based, understanding of the molecular details of the construction and operation of the catalyst and the economic and environmental importance of the discovery of more efficient abiological catalysts for the reactions catalysed so efficiently by the enzymes.

2. Recent applications of X-ray spectroscopy to nitrogenase

Less than half global nitrogen fixation, the conversion of inert dinitrogen into a form available to biology and industry, proceeds by the high-temperature/high-pressure Haber–Bosch process at a cost of ca. 1% of global human energy production (Rubio and Ludden, 2008; Smith, 2002). Nitrogenase enzymes contribute the remainder in a process that proceeds at room temperature and pressure. Knowledge of the remarkable iron–molybdenum cofactor (FeMo-co), the catalytic centre of nitrogenase, mostly derives from the crystal structures published by Rees and coworkers shown in Fig. 1 (Einsle et al., 2002; Kim and Rees, 1992a,b; Kim et al., 1993). It is noteworthy that the initial crystal structures failed to identify the presence of the central light atom (owing to issues to do with Fourier truncation), where this matter was only resolved with the availability of the 1.16 Å resolution structure (Einsle et al., 2002). Additional insights into the structure of FeMo-co and its chemistry under turnover conditions have been obtained from application of spectroscopic techniques including EPR, Mössbauer, IR and extended X-ray absorption fine structure (EXAFS) (Chen et al., 1993; Christiansen et al., 1995; Christie et al., 1996; Corbett et al., 2005; Di Cicco, 2003; Flank et al., 1986; Garner et al., 1989; George et al., 2008; Harvey et al., 1990, 1998;

* Corresponding author. Tel.: +61 3 83446505; fax: +61 3 93475180.
E-mail address: spbest@unimelb.edu.au (S.P. Best).

0969-806X/$ - see front matter Crown Copyright © 2009 Published by Elsevier Ltd. All rights reserved.
doi:10.1016/j.radphyschem.2009.03.072

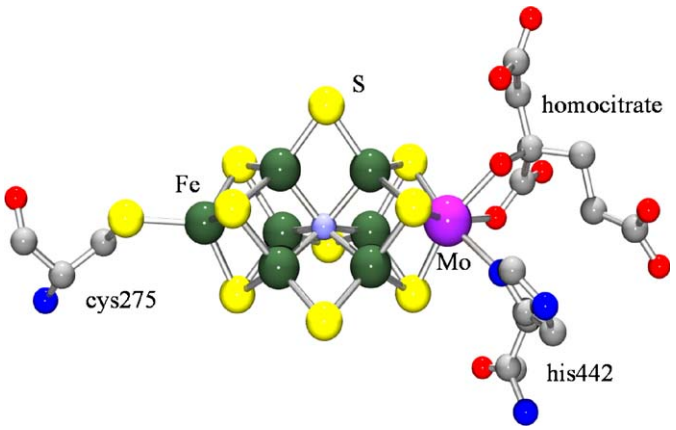

Fig. 1. Structure of FeMo-co, the catalytic site of the nitrogenase enzyme, as determined from the 1.16 Å structure, 1M1N (Einsle et al., 2002). The central atom is shown as N, but may be C or O. The 7FeMo9S cluster is bound to a homocitrate cofactor and is tethered to the protein by coordinate links to cysteinyl (Fe) and histidine (Mo) residues.

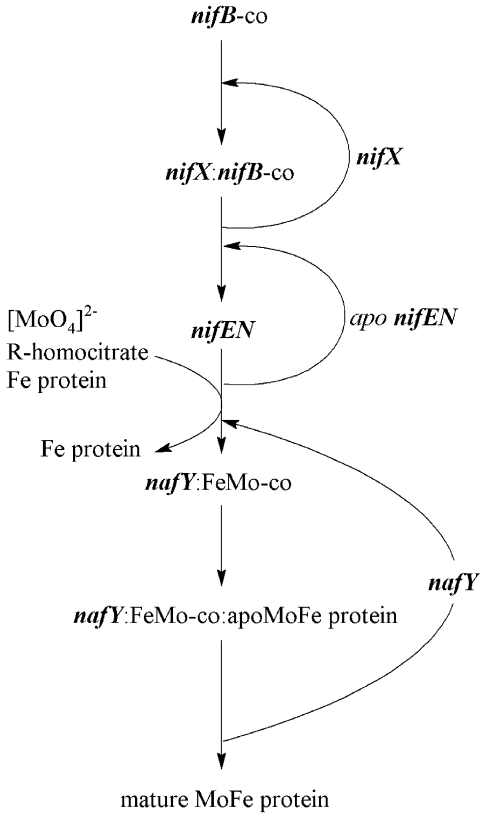

Fig. 2. Proposed biosynthetic sequence for formation of FeMo-co and its insertion into apo-MoFe protein (George et al., 2008; Rubio and Ludden, 2008).

Liu et al., 1994; Peters et al., 1998; Schunemann and Winkler, 2000; Strange et al., 2003).

An elegant example of the application of X-ray spectroscopy to complex molecular systems is provided by the recent investigation of the biosynthesis of FeMo-co (George et al., 2008). A series of ***nif*** genes have been identified as providing the proteins needed for synthesis of FeMo-co and its insertion into apo-MoFe protein and the proposed sequence of biosynthetic steps is summarised in Fig. 2 (Allen et al., 1994; Hu et al., 2005; Rubio and Ludden, 2008). The extent of formation of the MoFeS core and, more particularly, the incorporation of the central pinning light atom require analysis of the proteins formed at the different stages of the process. Whereas the presence, or absence, of the molybdenum atom in the clusters contained within the ***nif*** proteins is easily established with reference to the absorption at the molybdenum edge (Christiansen et al., 1995), determination of the number of iron atoms comprising the cluster and the presence of the central light atom present significantly greater challenges. Fe K-edge EXAFS of the ***nifX***:***nifB***-co and ***nafY***:FeMo-co precursors to the mature MoFe protein were analysed in terms of 6Fe, 7Fe and 8Fe models where in each case a nitrogen atom was included in the centre of a trigonal pyramidal arrangement of iron atoms (George et al., 2008). While small differences are obtained for the quality of the fits and values of certain Debye–Waller factors, each of the models give satisfactory values of the short Fe–S, short Fe–Fe and long Fe–Fe distances. Whereas correlation between the Fe–N and Fe–S distances was reported, search profiles obtained from fitting the EXAFS of ***nifX***:***nifB***-co using a 6Fe model with different fixed Fe–N distances and N atom population were shown to provide shallow minima with a population of 1.0 and a distance of 2.0 Å.

While more careful analysis of the EXAFS data will provide more reliable extraction of structural parameters (Chantler, 2008), the extent of the analysis is limited by the relatively poor information content of the EXAFS data. An important aspect of EXAFS studies of complex multinuclear targets is the integration of results from other techniques. In case of the study of FeMo-co precursors Cramer, Rubio and coworkers employed nuclear resonance vibrational spectroscopy (NRVS) using ^{57}Fe enriched samples (George et al., 2008). This technique involves measurement of the X-ray absorption spectrum with very highly monochromated X-rays (band width of 1.1 meV) at energies extending to ca. 60 meV from the $S=\frac{1}{2}$ to $\frac{3}{2}$ nuclear transition of ^{57}Fe (14.4125 keV) (Sturhahn, 2004). Separation of the much more intense electronic scattering, which has a natural lifetime of ca. 140 ns, from the required, but long-lifetime, nuclear scattering is achieved by using a pulsed source of X-rays and time gating the detector. The resulting spectrum gives a partial vibrational density of states weighted by the motion of the absorbing atom in the direction of the incident photon (Sturhahn, 2004). The extraction of useful information from experiments of this sort is strongly connected to the ability to assign the spectra features to particular normal modes. Recent advances in density functional theory (DFT) have allowed the calculation of the equilibrium geometries of complex metal-based systems together with the infrared (and Raman) spectra with a remarkably high level of agreement with experimental observations (Borg et al., 2007; Tye et al., 2006). Since the displacement coordinates for each of the atoms involved in the normal modes are calculated, the NRVS can be straightforwardly obtained (Petrenko et al., 2007). A combination of EXAFS, DFT and NRVS provides a powerful means of obtaining reliable structural information from the system. The inter-nuclear contacts obtained from EXAFS analysis may be used to assess the reliability of the DFT calculations which, in turn, may be used to calculate the NRVS. For the case in question, the reliability of the conclusion that the 6Fe model applies in the case of the ***nifX***:***nifB***-co complex is greatly enhanced by the consistency of the conclusions derived from EXAFS and NRVS analysis and DFT calculations. Moreover, the presence of the central light (nitrogen) atom is strongly supported by bands at 185–200 cm^{-1} in the NRVS spectrum which are interpreted as being a set of cluster "breathing" modes which are also observed in FeMo-co (George et al., 2007, 2008).

3. Recent applications of X-ray spectroscopy to hydrogenase

Whereas the turnover frequencies of nitrogenase enzymes are low, hydrogenase enzymes facilitate dihydrogen activation at fast

rates and with high efficiency (Vignais and Billoud, 2007). In this context, efficiency relates to the difference in potential between that for the reaction under catalysis and the potential for which the reaction occurs at a useful, mass transport limiting, rate. Elucidation of the molecular details of enzymatic dihydrogen activation is driven both by curiosity and practical reasons, where the latter reflect the need to discover catalysts for various types of hydrogen fuel cells. An important case in point concerns the anode of fuel cells suitable for transport applications. Whereas the proton exchange membrane fuel cells are sufficiently compact and have low operating temperatures, the platinum required as a catalyst for dihydrogen activation is simply not available in sufficient quantity to allow such cells to power a significant fraction of the annual vehicle production.

Three distinct forms of hydrogenase have been identified, where two of these facilitate reversible oxidation of dihydrogen or reduction of protons and the third that catalyses dihydrogen addition to a specific substrate, methynenyl–H_4MPT^+. This latter hydrogenase was known variously as MPT-, iron cluster free- or, simply, [Fe]-hydrogenase as the structure of the protein and its catalytic centre became more clearly defined. The first X-ray structure of the protein, including the metal cofactor, was published in 2008 (Shima et al., 2008) and this together with EXAFS and NRVS (Guo et al., 2008) studies reveals an unusual iron centre with bound carbon monoxide. Owing to the limited resolution able to be obtained for the protein X-ray structural analysis (1.75 Å), EXAFS analysis plays vital roles in assessment and development of the structural models and has a front-line role in the delineation of the chemistry of the system with inhibitors and substrate (Penner-Hahn, 2005; Zhang et al., 1999).

The two main classes of hydrogenase are of more relevance to applications involving consumption or generation of dihydrogen and these are classified in terms of the metals that comprise the catalytic centre and are known as the [NiFe]- and [FeFe]-hydrogenases (Adams, 1990; Cammack et al., 2001; Evans and Pickett, 2003). The crystal structures of both forms have been known for about 10 years (Fontecilla-Camps et al., 2007; Nicolet et al., 1999; Peters et al., 1998; Volbeda et al., 1995), and while the general features of the catalytic sites are known, the mechanistic details of the reaction and some aspects of the structure remain to be resolved (Pandey et al., 2008). It has been noted that whilst the three forms of hydrogenase are distinct in an evolutionary sense all three include iron centres with remarkably similar local geometries, including the incorporation of cyanide and/or carbon monoxide (Shima et al., 2008). Whilst common in co-ordination chemistry these ligands are highly unusual in biology.

An important aspect of the chemistry of the enzyme, relevant to its application in biotechnology, is its high sensitivity to dioxygen, in most cases resulting in permanent or temporary loss of activity. Reactivation of [NiFe]-hydrogenases occurs slowly on exposure to dihydrogen (De Lacey et al., 2007). In the enzyme, the polypeptide matrix helps protect the highly sensitive catalytic centre, this being located near the centre of the ca. 64 kDa proteins. For both [NiFe]- and [FeFe]-hydrogenases electron transport to and from the active site is mediated via a series of regularly spaced iron sulfur clusters and this is illustrated by the structure of the [FeFe]-hydrogenase (Fig. 3). Discovery of dioxygen-tolerant forms of the [NiFe]-hydrogenase has been exploited with the construction of a membrane-free hydrogen–oxygen fuel cell which utilizes carbon electrodes modified by adsorption of [NiFe]-hydrogenase at the anode and the dioxygen activating enzyme laccase adsorbed on the cathode (Vincent et al., 2007). The cell is able to operate with both electrodes exposed to air doped with 3% dihydrogen. While such devices may ultimately be useful for low-current applications, based on the normal current densities achieved in those

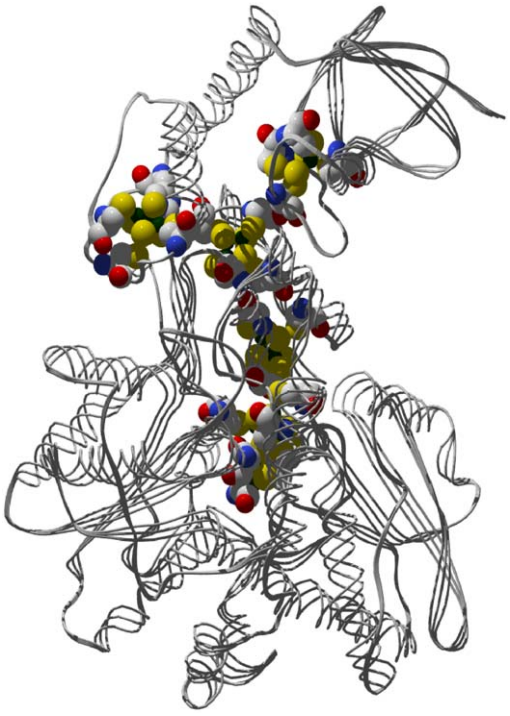

Fig. 3. Structure of [FeFe]-hydrogenase of *Clostridium pasteurianum* from 3C8Y (Pandey et al., 2008). The iron–sulfur clusters are shown as spacefilling representations and the protein backbone is shown in ribbon form. The active site is the lowermost iron–sulfur cluster.

experiments approximately half a tonne of enzyme would be required to power a moderate-sized car. The challenge that remains is the translocation of the enzyme chemistry to a form more amenable to large current applications. Clearly, one approach to the problem is to build the catalyst starting from the metal cofactor at the active site, i.e., to focus on the chemistry of metal complexes with structures, compositions and reactivity related to the active centres of the [NiFe]- and [FeFe]-hydrogenases.

While the compositon and structure of the active site provides a starting point for construction of biomimetic complexes, functional models must replicate the reaction chemistry. In this regard, knowledge of the reaction path is of critical importance. DFT methods have been used to consider the viability of the different reaction paths for dihydrogen activation by the diiron subsite of the [FeFe] hydrogenase H-cluster, Fig. 4 (Siegbahn et al., 2007). Two alternative pathways for the reaction may be considered; the first involves dihydrogen binding to the labile binding site occupied by the water molecule in Fig. 4 or, alternatively, dihydrogen binding at the site initially occupied by the bridging CO group. The two proposed pathways have been examined in a series of calculations comparing the energy difference between for dihydrogen activation/proton reduction (Zampella et al., 2006). In these studies, the 4Fe4S cube is replaced by a methyl group and the influence of the local environment is treated using a continuum solvation model with the calculations repeated with values of dielectric constant ranging between 0 and 40. Only the results obtained with $\varepsilon = 40$ are reported herein. These calculations of the reaction path place an N atom in the centre of the dithiolate bridge. Proton transfer between the protein environment and $\{FeFe\}_H$ was modelled by inclusion of a butylamine molecule which takes the place of a lysine residue in the enzyme.

The proposed reaction path for dihydrogen activation and proton reduction involving only terminally bound hydride is

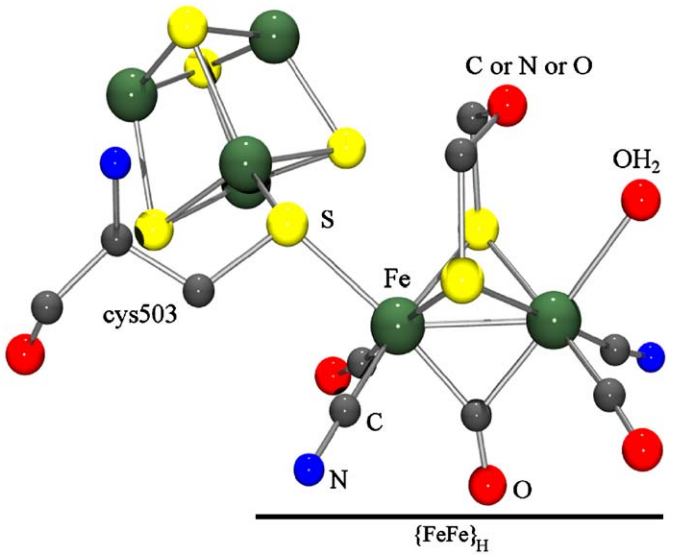

Fig. 4. The oxidized form of the [FeFe]-hydrogenase catalytic centre or H-cluster (drawn using coordinates from 3C8Y) (Pandey et al., 2008). The central atom of the bridging dithiolate of the diiron subsite, $\{FeFe\}_H$, is either C or N or O.

summarised in Scheme 1a. Dihydrogen cleavage and transfer of a proton to the N atom of the azadithiolate bridge (4→3 in Scheme 1a) is calculated to be thermodynamically favourable ($\Delta G = -7.7$ kcal/mol) and to have a low activation energy of 0.1 kcal/mol (Zampella et al., 2006); these calculations are consistent with previous reports (Fan and Hall, 2001; Liu and Hu, 2002a,b). The alternate reaction path involves dihydrogen binding opposite the bridging dithiolate and this is summarised in Scheme 1b. Breaking the H–H bond (14→12→11 in Scheme 1b) is also thermodynamically favourable ($\Delta G = -20.5$ kcal/mol) and has a calculated energy barrier less than 0.5 kcal/mol.

The reaction path for dihydrogen activation by [FeFe] hydrogenase serves to highlight both the strengths and limitations of the *ab initio* calculations. Improvements in the quality of the calculations and the ability to treat reliably transition-metal clusters, together with methods that allow for more realistic treatment of the protein H–cluster interface, by combining *ab initio* and molecular mechanics approaches (Greco et al., 2007a), mean that the viability of different reaction paths may be reasonably assessed on the basis of the calculated energetics. While this approach allows the exclusion of unfeasible reaction paths, it is more difficult to make a clear distinction between viable paths. Whereas the reaction path for dihydrogen activation by [FeFe] hydrogenase involving terminally bound hydrides (Scheme 1a) gives a lower activation energy than that obtained for a path involving bridging hydrides (Scheme 1b), the latter path is still viable. Moreover, a key underlying assumption of the calculations is that $\{FeFe\}_H$ includes a bridging azadithiolate. Should this not be correct, as has recently been suggested (Pandey et al., 2008), then the balance would tip strongly in favour of the bridging hydride. It is critically important that the experimentally based understanding of the enzyme and, as discussed in the following section, analogous chemical models be clearly defined. X-ray techniques are at the forefront of the approaches that will yield this information.

3.1. [FeFe] hydrogenase model chemistry

Since publication of the X-ray crystal structure of [FeFe] hydrogenase rapid advances have been achieved in terms of the design and synthesis of compounds that feature key elements of the diiron subsite of the catalytic centre, $\{FeFe\}_H$ (Fig. 4). In most cases, the compounds have been characterized by X-ray crystallography and recent reviews provide a good overview of the field (Liu et al., 2005). The doubly bridged diiron compounds are most simply represented by $Fe_2(\mu\text{-}S(CH_2)_3S)(CO)_6$, **3S**, where region-specific cyanation (Cloirec et al., 1999; Lyon et al., 1999; Schmidt et al., 1999) and replacement of the central atom of the dithiolate bridge by either NR (Li and Rauchfuss, 2002) or O (Song et al., 2004) gives a closer representation of $\{FeFe\}_H$. The 2Fe3S core geometry has been provided by elaboration of the bridging dithiolate (Lawrence et al., 2001; Razavet et al., 2001), where the full 6Fe core of the H-cluster has been achieved by linking a 4Fe4S cluster to the diiron fragment by a thiolate bridge (Tard et al., 2005). More recent work has focused on the identification of compounds that include a bridging CO group. X-ray structures have been reported for the oxidized ($Fe^{II}Fe^{I}$) analogues of $\{FeFe\}_H$ (Justice et al., 2007a; Liu and Darensbourg, 2007) and spectroscopic and computational evidence is available for CO-bridged analogues of the reduced $Fe^{I}Fe^{I}$ form (Cheah et al., 2007b).

3.2. Electrocatalytic proton reduction by H-cluster model compounds

In addition to the structural relationship between the diiron compounds, described above, and $\{FeFe\}_H$ a number of these compounds have been shown to catalyse proton reduction, albeit at potentials more negative than that of the enzyme (Capon et al., 2005). The most detailed studies of the electrocatalytic reaction have been completed for **3S** under conditions, where the initial reduction product is protonated by the acid (Borg et al., 2004). Simulation of the electrochemical response allows identification of the sequence of protonation and redox reactions (Scheme 2). An important characteristic of the electrocatalytic reaction of both the enzyme and **3S** is poisoning of the catalyst by CO. Inhibition of catalytic activity by CO is potentially a serious practical problem for hydrogen fuel cell catalysts particularly since dihydrogen obtained from hydrocarbons by the water shift reaction will be contaminated with CO.

Understanding of the impact of additional CO on the catalytic proton reduction by **3S** has depended on identification of the structure of the reaction products. In this case, crystals of the reduced products suitable for structural analysis were unavailable and structural elucidation required the integration of spectroscopic (IR, UV–vis), EXAFS and computational results (Bondin et al., 2006a,b; Borg et al., 2007). The structure of the side product and the reaction path leading to its formation is shown in Scheme 3, where subsequent investigations lead to crystallographic characterization of the dimeric product (Aguirre de Carcer et al., 2006).

Optimization of the catalyst involves both enhancement of the reaction of interest and inhibition of side reactions. Whereas the analogue of **3S** with a two-carbon linker between the bridging S atoms, **2S**, exhibits similar electrochemistry and electrocatalysis as **3S**, catalytic activity is not diminished by exposure to CO. For **2S** one-electron reduction also leads to dimer formation although the structure is different from $\mathbf{3S}_2^{2-}$ (Scheme 3) and is less susceptible to fragmentation in the presence of CO. Accordingly, the electrocatalytic response of **2S** is not subject to poisoning in the presence of CO. The structures of the dimer formed by $\mathbf{2S}^{1-}$ and the reaction products formed have been elucidated by a combination of IR spectroscopy, EXAFS and DFT (Borg et al., 2004).

While there has been some success in identifying the side products formed during reduction of $\{FeFe\}_H$ model compounds in the presence and absence of acid, identification of the reduced protonated species involved in the catalytic cycle has proved to be

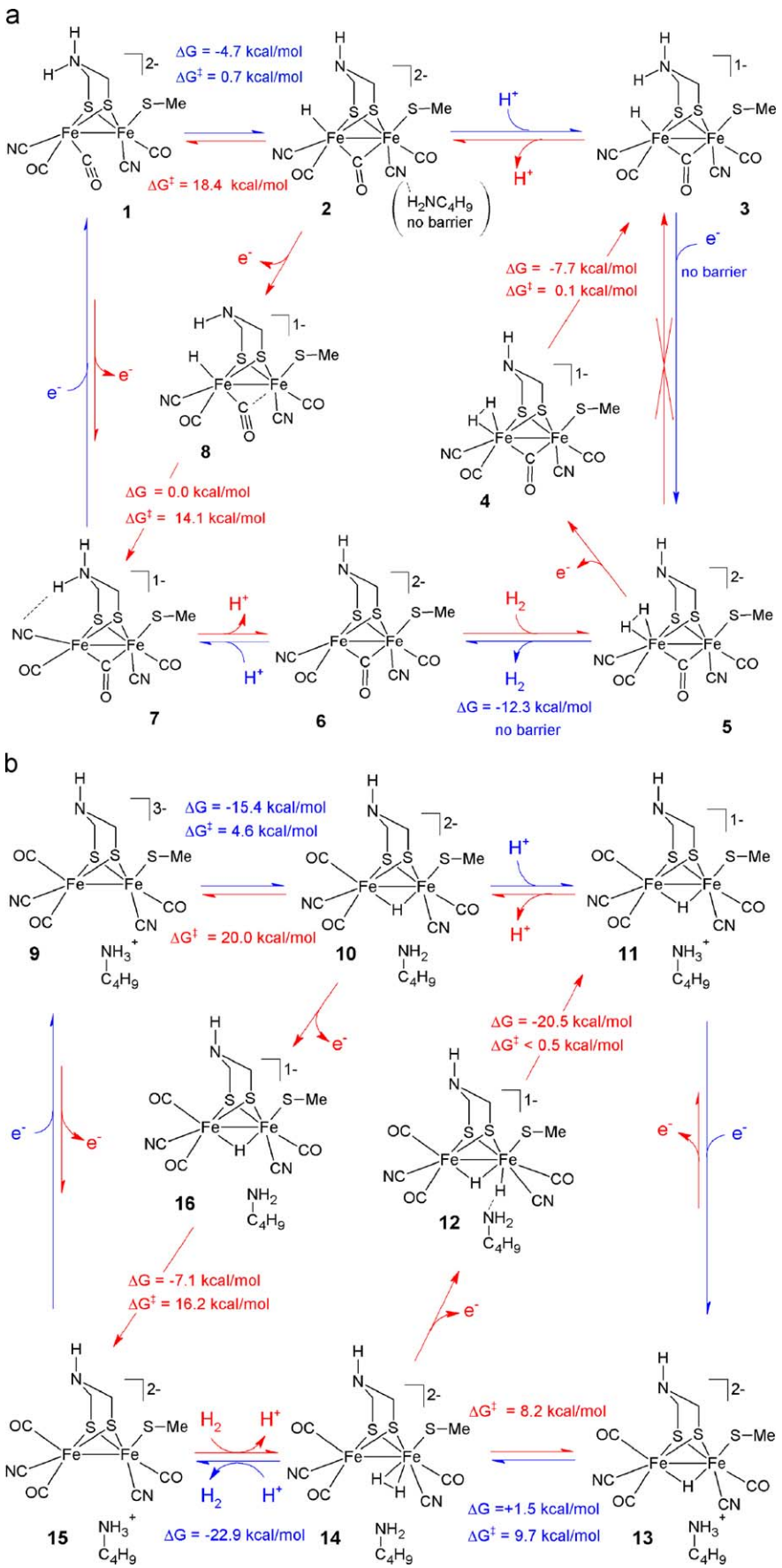

Scheme 1. Summary of the DFT-calculated reaction paths for dihydrogen activation (inner arrows, red) and proton reduction (outer arrows, blue) involving (a) terminally bound hydrides and (b) bridging hydrides. The values of ΔG and $\Delta G^{\ddagger}$ corresponds to calculations with $\varepsilon = 40$ and the numbering scheme for the different structures follows that used in the original publication (Zampella et al., 2006). (For interpretation of the references to colour in this figure legend, the reader is referred to the web version of this article).

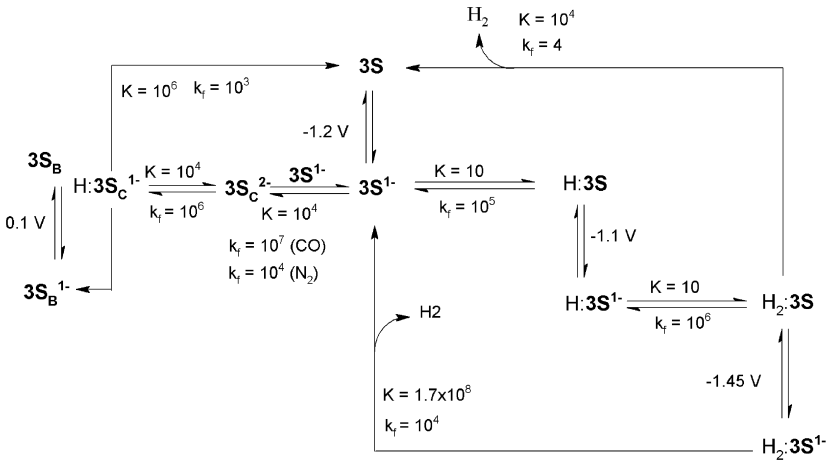

Scheme 2. Reaction path for electrocatalytic proton reduction by **3S** in presence of *p*-toluenesulfonic acid (Borg et al., 2004).

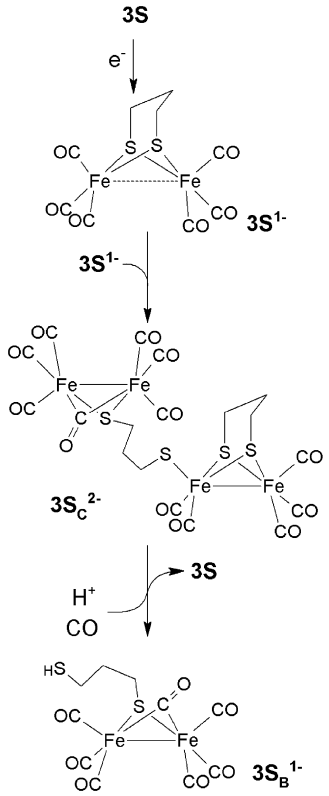

Scheme 3. Proposed reduction chemistry of **3S** based on spectroscopic and EXAFS observations.

more problematic. In this case, DFT methods have used to explore the possible structures of the protonated reduced species and provide estimates of the reduction potentials and reaction rates (Greco et al., 2007b). The conclusions of that study are summarised in Scheme 4. In addition to providing support for the reaction sequence deduced from the electrochemical simulations (Scheme 2) the calculations indicate that dihydrogen formation from these highly reduced compounds proceeds via bridging hydrides, analogous to Scheme 1b for the enzyme, with the pathway involving terminally bound hydrides computed to be far less favourable (Greco et al., 2007b). Support for the proposition that electrocatalytic proton reduction proceeds through bridged hydrides is provided by studies of the phosphorus-bridged analogue of **3S**, $Fe_2(\mu\text{-}PhP(CH_2)_3PPh)(CO)_6$, **3P**. In this case, reduction proceeds in two closely spaced one-electron steps where EXAFS, DFT and IR characterization of **3P**, $\mathbf{3P}^{-}$ and $\mathbf{3P}^{2-}$ has been reported (Cheah et al., 2007a). In common with **3S**, **3P** supports electrocatalytic proton reduction at the two-electron level, albeit at a lower rate. Calculations of the doubly reduced, doubly protonated analogue of **3P** suggest a structure analogous to that of $\mathbf{H_2 3S}$ (Scheme 4) although in that case the 2Fe2P core geometry results in a calculated H–H distance of 2.067 Å. For $\mathbf{H_2 3S}$, the corresponding calculated H–H distance of 1.760 Å is closer to the transition state and provides an explanation for the difference in rates of electrocatalytic proton reduction by **3S** and **3P**. While the preceding arguments are based on calculations of the geometry of the doubly protonated species, a more compelling link between the reactivity of dihydrides of structure analogous to $\mathbf{H_2 3S}$, and the H–H distance is provided by the chemistry of $Fe_2(\mu\text{-}PPh_2)_2(CO)_6$; **DP**. Reduction of **DP** proceeds to give a dianion with a planar 2Fe2P core with a long Fe–Fe distance of 3.360 Å (Ginsburg et al., 1979). Protonation of $\mathbf{DP}^{2-}$ has been shown to give a moderately stable product with an IR spectrum matching that expected for protonation at both of the weakly interacting Fe atoms (Cheah et al., 2004). The long Fe–Fe separation precludes formation of bridging hydrides. A structure analogous to $\mathbf{H_2 3S}$ (Scheme 4) but with a planar 2Fe2P core is calculated for $\mathbf{H_2 DP}$, where this structure is supported by the close agreement between the observed and calculated IR spectra (Cheah et al., 2007a). Further, details of the DFT calculated structure such as the Fe–Fe and Fe–CO distances, including differences for the CO groups adjacent and opposite the hydride, are reproduced in our preliminary EXAFS analysis of this product (Cheah, 2008).

3.3. *Influence of protonation on the 2Fe2S core geometry*

Given that the catalytic reaction of interest involves proton reduction/dihydrogen oxidation it is clearly important to focus on $\{FeFe\}_H$ model compounds bound to either the reactant or product of the reaction. While there are no well-defined dithiolate-bridged diiron compounds that include dihydrogen (Kubas, 2007), there is a reasonably broad literature now available for the protonated species. Protonation of electron-rich analogues of **3S** proceeds readily where the spectroscopy and X-ray structural evidence point clearly to the formation of bridged hydrides with structures analogous to **H3S** (Scheme 4) (Zhao et al., 2002). The preference for bridging hydrides is well reflected by DFT calculations which typically show a 10 kcal/mol energy difference between isomers

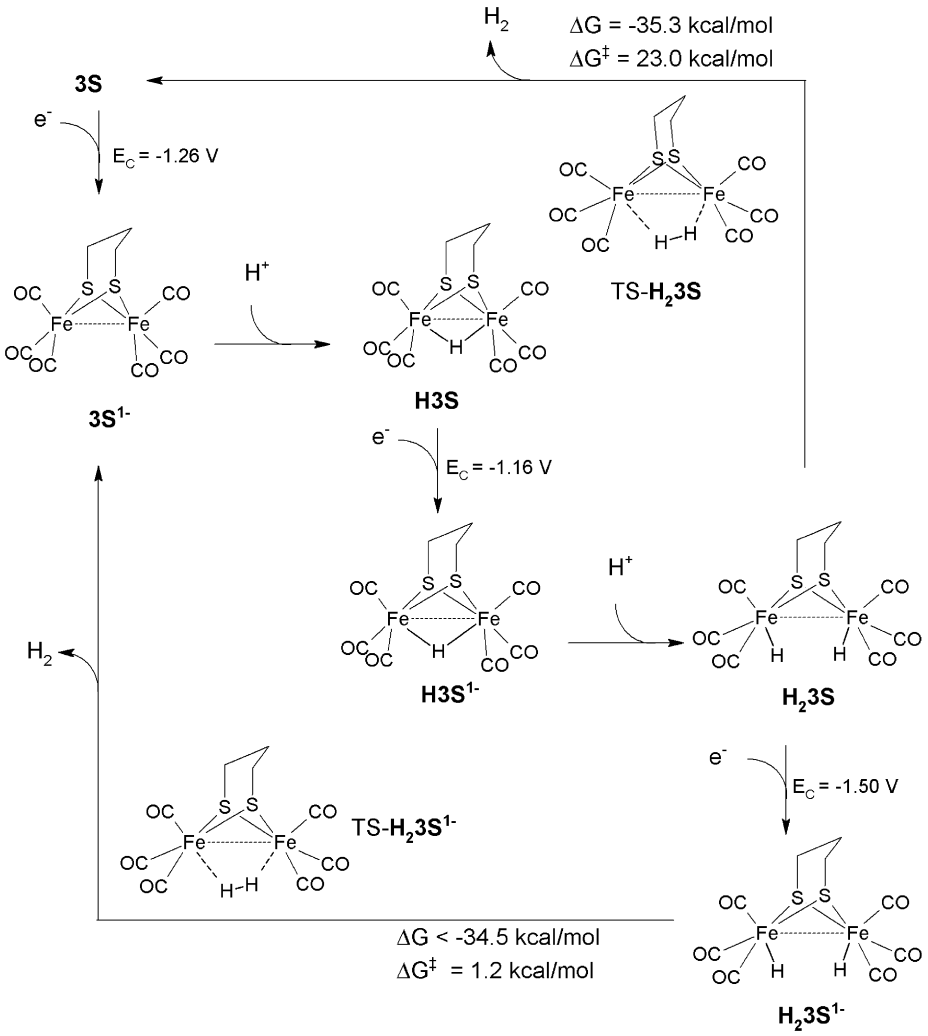

Scheme 4. DFT calculated reaction path for electrocatalytic proton reduction by **3S** (Greco et al., 2007b).

having a bridging hydride and the form including a bridging CO group and a terminally bound hydride (Cao and Hall, 2001; Siegbahn et al., 2007; Zampella et al., 2006). It is surprising that there is increasing evidence that the thermodynamic product having a bridging hydride is formed from a kinetic product that involves a terminally bound hydride (Adam et al., 2008; Barton and Rauchfuss, 2008; Ezzaher et al., 2008, 2007).

Evidence for a markedly different reactivity for the terminally bound and bridging hydrides is obtained from studies of the products of hydride reaction with the $Fe^{II}Fe^{II}$ compound $[Fe_2(\mu\text{-}S(CH_2)_2S)(PMe_3)_4(CO)_2]^{2+}$ (van der Vlugt et al., 2005). In this case, the kinetic product was fully characterized and shown to have terminally bound hydride and bridging CO groups and, importantly, reacts readily with protons to eliminate dihydrogen. The thermodynamic product has a bridging hydride and this compound is unreactive with protons (van der Vlugt et al., 2005). While reliant only on spectroscopic and DFT evidence similar conclusions are drawn for a tetra-iron compound that, on reduction and protonation, gives diiron fragments with a bridging CO group and a terminally bound hydride. This species undergoes electrocatalysis at rates ca. 1000 times faster than **3S** (Cheah et al., 2007b).

In many cases, the products of the protonation reactions are unstable and in these instances EXAFS presents the best opportunity to obtain direct structural information that may be used to exaluate the DFT calculations. A recent study of the protonated forms of $Fe_2(\mu\text{-}(SCH_2)_2N(CH_2Ph))(PMe_3)_2(CO)_4$, $\mathbf{PS_{NR}}$, highlights the subtlety of the system (Löscher et al., 2007). In this case, protonation can occur at the Fe–Fe bond, the bridging N atom or at both sites Scheme 5). EXAFS collected from the neutral compound and from each of the three protonated species allow extraction of structural information including the Fe–Fe separation. Protonation of $\mathbf{PS_{NR}}$ with one equivalent of strong acid results in protonation of the N atom of the bridging dithiolate (Scheme 5) and this results in a surprisingly large increase in the Fe–Fe contact. DFT calculations of the system suggest that associated with protonation is a rotation of the co-ordination sphere of one of the iron atoms to move the apical PMe_3 group to a basal position. In addition to the changes in electronic and molecular structure associated with the rearrangement of the phosphine, there is an additional "hydrogen-bonding" interaction between the NH and apical CO group. It is the change in conformation of the PMe_3 groups that appears to be associated with a significant lengthening of the FeFe distance (Löscher et al., 2007).

Whereas the EXAFS provides information in the structural changes attendant on protonation of $\mathbf{PS_{NR}}$, the X-ray absorption near-edge spectra (XANES) provides insights into the electronic structure of the absorbing atom where this, of course, is highly sensitive to the co-ordination geometry. Significant differences in the XANES are obtained for $\mathbf{PS_{NR}}$ and each of the protonated species (Löscher et al., 2007).

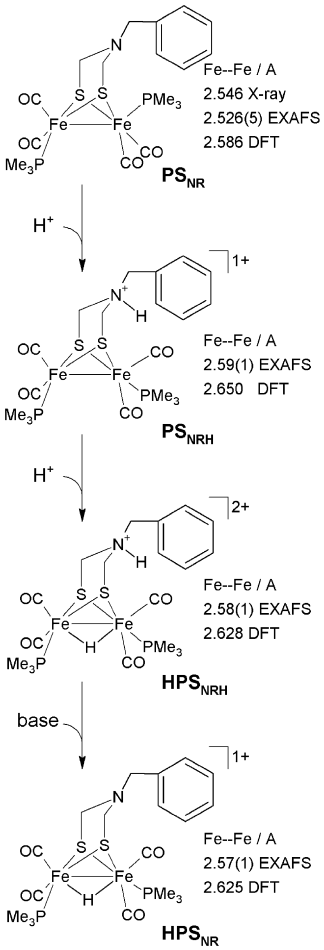

Scheme 5. Summary of the protonation reactions of **PSNR** as deduced from EXAFS and DFT calculations (Löscher et al., 2007).

These investigations highlight the complementarity of DFT calculations and X-ray spectroscopy (EXAFS and XANES) and the means by which they can provide reliable estimates of the molecular and electronic structure and a framework for understanding those results.

3.4. *Asymmetry of the iron co-ordination environment of 2Fe2S*

The co-ordination environment of the Fe atoms of $\{FeFe\}_H$ is clearly different (Fig. 4) from that of the 2Fe2S model compounds and there is a strong suggestion that this makes an important contribution to the chemistry of the system. In the reduced, Fe^IFe^I, form of $\{FeFe\}_H$ the bridging CO group moves to a position closer to the Fe atom linked to the 4Fe4S cube (Fig. 4). DFT calculations suggest a significant Fe^0Fe^{II} character for this geometry (Fiedler and Brunold, 2005), a factor that may favour formation of a terminally bound hydride.

Clearly, asymmetry can be built into the $\{FeFe\}_H$ model compounds by differences in the substitution pattern of the groups bound to the diiron core as, for example, in the cases where there is a 2Fe3S core composition as mentioned in Section 3.1. It is important to note, however, that the normal substitution reactions of electron-rich substituents proceed to replacement of two CO groups, one on each Fe centre, to give a symmetrically substituted product. By the use of bidentate ligands such as $PPh_2(CH_2)_2PPh_2$ it is possible to isolate useful yields of the diiron compounds with two CO groups on a single Fe centre replaced by the bidentate ligand (Adam et al., 2008; Ezzaher et al., 2007, 2008; Gao et al., 2007; Justice et al., 2007b). In these cases protonation leads, initially, to formation of a terminal hydride that undergoes slow rearrangement to the more stable bridging hydride form (Adam et al., 2008; Ezzaher et al., 2007). While these compounds have not been shown to react further with acid to eliminate dihydrogen they provide a strong link to the reaction path proposed for $\{FeFe\}_H$, where protonation gives a terminally bound hydride (Scheme 1a). In the case of the H-cluster electron transfer from the 4Fe4S cluster enhances the hydridic character of the complex and allows dihydrogen elimination on protonation. Spectroscopic and DFT studies of the reduction chemistry of $Fe_4((\mu\text{-}SCH_2)_3CCH_3)_2(CO)_8$, **4Fe6S**, suggests that two-electron reduction leads to rearrangement to give diiron fragments with a bridging CO group (Cheah et al., 2007b). The formal oxidation states of the Fe atoms of $\mathbf{4Fe6S^{2-}}$ are $Fe^{II}Fe^0$, analogous to the reduced form of $\{FeFe\}_H$. The high rate of electrocatalytic proton reduction found for **4Fe6S** indicates that the hydride formed in that instance is reactive, presumably because of the availability of an additional electron from the second diiron fragment. Should these conclusions prove to be correct **4Fe6S** would represent a functioning system with a reaction path analogous to Scheme 1a.

At this time, the X-ray spectroscopy of the asymmetrically substituted diiron compounds, including 4Fe6S, is poorly explored. It will be important to develop our understanding of the electronic and molecular structure about the individual Fe atoms. Application and development of techniques such as site selective EXAFS (Glatzel et al., 2002) and crystallographic studies using multiple wavelengths near the Fe edge (Einsle et al., 2007) may provide the critical insights needed to deepen the understanding of these comparatively simple systems.

4. Concluding remarks

Just as transition metals appear to be perfectly suited to act as the catalytic centres of enzymes, synchrotron X-radiation is perfectly suited to the study of transition metals. The delineation of the protein and cofactor structure (X-ray diffraction), the local co-ordination geometry about the metal (EXAFS) through to the electronic (XANES) and vibrational (NVRS) structure are all addressed using X-rays. Both in terms of the analysis of the results and from the perspective of providing an intellectual framework for understanding the physics and chemistry of the system it is critical to integrate X-ray studies with other techniques. For transition-metal systems, the impact of DFT techniques cannot be overstated. For the $\{FeFe\}_H$ model compounds, IR spectroscopy plays an important role because the intense ν(CO) bands are sensitive to the electron richness of the metals to which they are bound and the pattern of bands is sensitive to the details of the structure of the compound. Accordingly, the marriage of EXAFS, DFT and IR spectroscopy allows reliable structure identification of the reactive compounds formed following reduction and/or protonation. Knowledge of these compounds is essential for an understanding of the reaction path for the catalytic and electrocatalytic reactions and with that the tools needed to engage in rational development of the catalysts needed to drive forward key areas of industry and technology.

Acknowledgments

SPB gratefully acknowledges the Australian Research Council for funding related research. M-HC gratefully acknowledges the University of Melbourne for the award of a scholarship. Our

previous EXAFS experiments were performed at the Australian National Beamline Facility with support from the Australian Synchrotron Research Program, which is funded by the Commonwealth of Australia under the Major National Research Facilities Program. Support of the Victorian Institute for Chemical Sciences High Performance Computing Facility is gratefully acknowledged. Dr. K.A. Vincent, Dr. S.J. Borg and Dr. M.I. Bondin are thanked for their work in one or more of the areas discussed and Professor C.J. Pickett and his group are thanked for their chemistry and many stimulating discussions on FeMo-co and $\{FeFe\}_H$ model chemistry.

References

Adam, F.I., Hogarth, G., Kabir, S.E., Richards, I., 2008. Models of the iron-only hydrogenase: synthesis and protonation of bridge and chelate complexes $[Fe_2(CO)_4\{Ph_2P(CH_2)_nPPh_2\}(m\text{-pdt})]$ $(n=2–4)$ —evidence for a terminal hydride intermediate. Comptes Rendus Chimie 11, 890–905.

Adams, M.W.W., 1990. The structure and mechanism of iron-hydrogenases. Biochimica et Biophysica Acta 1020, 115–145.

Aguirre de Carcer, I., Di Pasquale, A., Rheingold, A.L., Heinekey, D.M., 2006. Active-site models for iron hydrogenases: reduction chemistry of dinuclear iron complexes. Inorganic Chemistry 45, 8000–8002.

Allen, R.M., Chatterjee, R., Madden, M.S., Ludden, P.W., Shah, V.K., 1994. Biosynthesis of the iron-molybdenum cofactor of nitrogenase. Critical Reviews in Biotechnology 14, 225–249.

Barton, B.E., Rauchfuss, T.B., 2008. Terminal hydride in [FeFe]-hydrogenase model has lower potential for H_2 production than the isomeric bridging hydride. Inorganic Chemistry 47, 2261–2263.

Bertini, I., Gray, H.B., Lippard, S.J., Valentine, J.S., 1994. Bioinorganic Chemistry.

Bondin, M.I., Borg, S.J., Cheah, M.-H., Best, S.P., 2006a. XAFS of short-lived reduction products of structural and functional models of the [Fe–Fe] hydrogenase H-cluster. Radiation Physics and Chemistry 75, 1878–1883.

Bondin, M.I., Borg, S.J., Cheah, M.H., Foran, G., Best, S.P., 2006b. Integration of EXAFS, spectroscopic, and DFT techniques for elucidation of the structure of reactive Diiron compounds. Australian Journal of Chemistry 59, 263–272.

Borg, S.J., Behrsing, T., Best, S.P., Razavet, M., Liu, X., Pickett, C.J., 2004. Electron transfer at a dithiolate-bridged assembly: electrocatalytic hydrogen evolution. Journal of the American Chemical Society 126, 16988–16999.

Borg, S.J., Tye, J.W., Hall, M.B., Best, S.P., 2007. Assignment of molecular structures to the electrochemical reduction products of Diiron compounds related to [Fe–Fe] hydrogenase: a combined experimental and density functional theory study. Inorganic Chemistry 46, 384–394.

Burgess, B.K., Lowe, D.J., 1996. Mechanism of molybdenum nitrogenase. Chemical Reviews 96, 2983–3011.

Cammack, R., Albracht, S.P.J., Armstrong, F.A., Bleijlevens, B., Faber, B., Fernandez, V.M.F., Hagen, W.R., Hatchikian, E.C., Jones, A.K., Pershad, H.R., 2001. Hydrogenases and their activities. In: Cammack, R., Frey, M., Robson, R.L. (Eds.), Hydrogen as a Fuel. Taylor & Francis, London, pp. 73–92 (pp. 238–261).

Cao, Z., Hall, M.B., 2001. Modeling the active sites in metalloenzymes. 3. Density functional calculations on models for [Fe]-hydrogenase: structures and vibrational frequencies of the observed redox forms and the reaction mechanism at the Diiron active center. Journal of the American Chemical Society 123, 3734–3742.

Capon, J.-F., Gloaguen, F., Schollhammer, P., Talarmin, J., 2005. Catalysis of the electrochemical H_2 evolution by di-iron sub-site models. Coordination Chemistry Reviews 249, 1664–1676.

Chantler, C.T., 2008. Accurate measurement and physical insight: The X-ray extended range technique for fundamental atomic physics, condensed matter research and biological sciences. Radiation Physics and Chemistry, this issue.

Cheah, M.H., 2008. Electrocatalysis by Diiron Analogues of the H-Cluster. PhD thesis, University of Melbourne, Melbourne.

Cheah, M.H., Borg, S.J., Best, S.P., 2007a. Steps along the path to dihydrogen activation at [FeFe] hydrogenase structural models: dependence of the core geometry on electrocatalytic proton reduction. Inorganic Chemistry 46, 1741–1750.

Cheah, M.H., Borg, S.J., Bondin, M.I., Best, S.P., 2004. Electrocatalytic proton reduction by Phosphido-bridged Diiron. Inorganic Chemistry 43, 5635–5644.

Cheah, M.H., Tard, C., Borg, S.J., Liu, X., Ibrahim, S.K., Pickett, C.J., Best, S.P., 2007b. Modeling [Fe–Fe] hydrogenase: evidence for bridging carbonyl and distal iron coordination vacancy in an electrocatalytically competent proton reduction by an iron thiolate assembly that operates through Fe(0)-Fe(II) levels. Journal of the American Chemical Society 129, 11085–11092.

Chen, J., Christiansen, J., Tittsworth, R.C., Hales, B.J., George, S.J., Coucouvanis, D., Cramer, S.P., 1993. Iron EXAFS of Azotobacter vinelandii nitrogenase molybdenum-iron and vanadium-iron proteins. Journal of the American Chemical Society 115, 5509–5515.

Christiansen, J., Tittsworth, R.C., Hales, B.J., Cramer, S.P., 1995. Fe and Mo EXAFS of Azotobacter Vinelandii nitrogenase in partially oxidized and singly reduced forms. Journal of the American Chemical Society 117, 10017–10024.

Christie, P.D., Lee, H.-I., Cameron, L.M., Hales, B.J., Orme-Johnson, W.H., Hoffman, B.M., 1996. Identification of the CO-binding cluster in nitrogenase MoFe protein by ENDOR of ^{57}Fe isotopomers. Journal of the American Chemical Society 118, 8707–8709.

Cloirec, A.L., Davies, S.C., Evans, D.J., Hughes, D.L., Pickett, C.J., Best, S.P., Borg, S., 1999. A di-iron dithiolate possessing structural elements of the carbonyl/cyanide sub-site of the H-centre of Fe-only hydrogenase. Chemical Communications, 2285–2286.

Corbett, M.C., Tezcan, F.A., Einsle, O., Walton, M.Y., Rees, D.C., Latimer, M.J., Hedman, B., Hodgson, K.O., 2005. Mo K- and L-edge X-ray absorption spectroscopic study of the ADP.AlF_4^--stabilized nitrogenase complex: comparison with MoFe protein in solution and single crystal. Journal of Synchrotron Radiation 12, 28–34.

De Lacey, A.L., Fernandez, V.M., Rousset, M., Cammack, R., 2007. Activation and inactivation of hydrogenase function and the catalytic cycle: spectroelectrochemical studies. Chemical Reviews 107, 4304–4330.

Di Cicco, A., 2003. Local structure in molecular complexes probed by multiple-scattering XAS. Journal of Synchrotron Radiation 10, 46–50.

Duhme-Klair, A.K., 2008. Bioinorganic chemistry. Annual Reports on the Progress of Chemistry, Section A: Inorganic Chemistry 104, 455–476.

Einsle, O., Andrade, S.L.A., Dobbek, H., Meyer, J., Rees, D.C., 2007. Assignment of individual metal redox states in a metalloprotein by crystallographic refinement at multiple X-ray wavelengths. Journal of the American Chemical Society 129, 2210–2211.

Einsle, O., Tezcan, F.A., Andrade, S.L.A., Schmid, B., Yoshida, M., Howard, J.B., Rees, D.C., 2002. Nitrogenase MoFe-protein at 1.16 Å resolution: a central ligand in the FeMo-cofactor. Science 297, 1696–1700.

Evans, D.J., Pickett, C.J., 2003. Chemistry and the hydrogenases. Chemical Society Reviews 32, 268–275.

Ezzaher, S., Capon, J.-F., Gloaguen, F., Kervarec, N., Petillon, F.Y., Pichon, R., Schollhammer, P., Talarmin, J., 2008. Diiron chelate complexes relevant to the active site of the iron-only hydrogenase. Comptes Rendus Chimie 11, 906–914.

Ezzaher, S., Capon, J.-F., Gloaguen, F., Petillon, F.Y., Schollhammer, P., Talarmin, J., Pichon, R., Kervarec, N., 2007. Evidence for the formation of terminal hydrides by protonation of an asymmetric iron hydrogenase active site mimic. Inorganic Chemistry 46, 3426–3428.

Fan, H.-J., Hall, M.B., 2001. A capable bridging ligand for Fe-only hydrogenase: density functional calculations of a low-energy route for heterolytic cleavage and formation of dihydrogen. Journal of the American Chemical Society 123, 3828–3829.

Fiedler, A.T., Brunold, T.C., 2005. Combined spectroscopic/computational study of binuclear Fe(I)-Fe(I) complexes: implications for the fully-reduced active-site cluster of Fe-only hydrogenases. Inorganic Chemistry 44, 1794–1809.

Flank, A.M., Weininger, M., Mortenson, L.E., Cramer, S.P., 1986. Single crystal EXAFS of nitrogenase. Journal of the American Chemical Society 108, 1049–1055.

Fontecilla-Camps, J.C., Volbeda, A., Cavazza, C., Nicolet, Y., 2007. Structure/function relationships of [NiFe]- and [FeFe]-hydrogenases. Chemical Reviews 107, 4273–4303.

Gao, W., Ekstroem, J., Liu, J., Chen, C., Eriksson, L., Weng, L., Akermark, B., Sun, L., 2007. Binuclear iron-sulfur complexes with bidentate phosphine ligands as active site models of Fe-hydrogenase and their catalytic proton reduction. Inorganic Chemistry 46, 1981–1991.

Garner, C.D., Arber, J.M., Hasnain, S.S., Dobson, B.R., Eady, R.R., Smith, B.E., 1989. X-ray absorption spectroscopic studies of the catalytic centers of nitrogenases. Physica B: Condensed Matter 158, 74–77.

George, S.J., Igarashi, R.Y., Piamonteze, C., Soboh, B., Cramer, S.P., Rubio, L.M., 2007. Identification of a Mo–Fe–S cluster on NifEN by MoK-edge extended X-ray absorption fine structure. Journal of the American Chemical Society 129, 3060–3061.

George, S.J., Igarashi, R.Y., Xiao, Y., Hernandez, J.A., Demuez, M., Zhao, D., Yoda, Y., Ludden, P.W., Rubio, L.M., Cramer, S.P., 2008. Extended X-ray absorption fine structure and nuclear resonance vibrational Spectroscopy reveal that NifB-co, a FeMo-co precursor, comprises a 6Fe core with an interstitial light atom. Journal of the American Chemical Society 130, 5673–5680.

Ginsburg, R.E., Rothrock, R.K., Finke, R.G., Collman, J.P., Dahl, L.F., 1979. The (metal-metal)-nonbonding $[Fe_2(CO)_6(m_2\text{-}PPh_2)_2]^{2-}$ dianion. Synthesis, structural analysis of its unusual dimeric geometry, and stereochemical-bonding implications. Journal of the American Chemical Society 101, 6550–6562.

Glatzel, P., Jacquamet, L., Bergmann, U., de Groot, F.M.F., Cramer, S.P., 2002. Site-selective EXAFS in mixed-valence compounds using high-resolution fluorescence detection: a study of iron in Prussian blue. Inorganic Chemistry 41, 3121–3127.

Greco, C., Bruschi, M., De Gioia, L., Ryde, U., 2007a. A QM/MM investigation of the activation and catalytic mechanism of Fe-only hydrogenases. Inorganic Chemistry 46, 5911–5921.

Greco, C., Zampella, G., Bertini, L., Bruschi, M., Fantucci, P., Gioia, L.D., 2007b. Insights into the mechanism of electrocatalytic hydrogen evolution mediated by $Fe_2(S_2C_3H_6)(CO)_6$, the simplest functional model of the Fe-hydrogenase active site. Inorganic Chemistry 47, 108–116.

Guo, Y., Wang, H., Xiao, Y., Vogt, S., Thauer, R.K., Shima, S., Volkers, P.I., Rauchfuss, T.B., Pelmenschikov, V., Case, D.A., Alp, E.E., Sturhahn, W., Yoda, Y., Cramer, S.P., 2008. Characterization of the Fe site in iron-sulfur cluster-free hydrogenase (Hmd) and of a model compound via nuclear resonance vibrational spectroscopy (NRVS). Inorganic Chemistry 47, 3969–3977.

Harvey, I., Arber, J.M., Eady, R.R., Smith, B.E., Garner, C.D., Hasnain, S.S., 1990. Iron K-edge X-ray-absorption spectroscopy of the iron-vanadium cofactor of the vanadium nitrogenase from Azotobacter chroococcum. Biochemical Journal 266, 929–931.

Harvey, I., Strange, R.W., Schneider, R., Gormal, C.A., Garner, C.D., Hasnain, S.S., Richards, R.L., Smith, B.E., 1998. X-ray absorption spectroscopic studies of the binding of ligands to FeMoco of nitrogenase from Klebsiella pneumoniae. Inorganica Chimica Acta 275–276, 150–158.

Hinnemann, B., Norskov, J.K., 2006. Catalysis by enzymes: the biological ammonia synthesis. Topics in Catalysis 37, 55–70.

Holland, P.L., 2004. Nitrogen fixation. Comprehensive Coordination Chemistry II 8, 569–599.

Howard, J.B., Rees, D.C., 2006. How many metals does it take to fix N_2? A mechanistic overview of biological nitrogen fixation. Proceedings of the National Academy of Sciences of the United States of America 103, 17088–17093.

Hu, Y., Fay, A.W., Ribbe, M.W., 2005. Identification of a nitrogenase FeMo cofactor precursor on NifEN complex. Proceedings of the National Academy of Sciences of the United States of America 102, 3236–3241.

Justice, A.K., Zampella, G., De Gioia, L., Rauchfuss, T.B., 2007a. Lewis vs. Bronsted-basicities of diiron dithiolates: spectroscopic detection of the ''rotated structure'' and remarkable effects of ethane-vs. Propanedithiolate. Chemical Communications, 2019–2021.

Justice, A.K., Zampella, G., De Gioia, L., Rauchfuss, T.B., van der Vlugt, J.I., Wilson, S.R., 2007b. Chelate control of diiron(I) dithiolates relevant to the [Fe–Fe]-hydrogenase ative site. Inorganic Chemistry 46, 1655–1664.

Kim, J., Rees, D.C., 1992a. Crystallographic structure and functional implications of the nitrogenase molybdenum-iron protein from Azotobacter vinelandii. Nature 360, 553–560.

Kim, J., Rees, D.C., 1992b. Structural models for the metal centers in the nitrogenase molybdenum-iron protein. Science 257, 1677–1682.

Kim, J., Woo, D., Rees, D.C., 1993. X-ray crystal structure of the nitrogenase molybdenum-iron protein from clostridium pasteurianum at 3.0-Å resolution. Biochemistry 32, 7104–7115.

Kubas, G.J., 2007. Fundamentals of H_2 binding and reactivity on transition metals underlying hydrogenase function and H_2 production and storage. Chemical Reviews 107, 4152–4205.

Lawrence, J.D., Li, H., Rauchfuss, T.B., 2001. Beyond Fe-only hydrogenases: N-functionalized 2-aza-1,3-dithiolates $Fe_2[(SCH_2)_2NR](CO)_x$ ($x = 5$, 6). Chemical Communications, 1482–1483.

Li, H., Rauchfuss, T.B., 2002. Iron carbonyl sulfides, formaldehyde, and amines condense to give the proposed azadithiolate cofactor of the Fe-only hydrogenases. Journal of the American Chemical Society 124, 726–727.

Liu, H.I., Burgess, B.K., Natoli, C.R., Filipponi, A., Gavini, N., Hedman, B., Di Cicco, A., Hodgson, K.O., 1994. EXAFS studies of FeMo-cofactor and MoFe protein: direct evidence for the long-range Mo–Fe–Fe interaction and cyanide binding to the Mo in FeMo-cofactor. Journal of the American Chemical Society 116, 2418–2423.

Liu, T., Darensbourg, M.Y., 2007. A mixed-valent, Fe(II)Fe(I), Diiron complex reproduces the unique rotated state of the [FeFe]hydrogenase active site. Journal of the American Chemical Society 129, 7008–7009.

Liu, X., Ibrahim, S.K., Tard, C., Pickett, C.J., 2005. Iron-only hydrogenase: synthetic, structural and reactivity studies of model compounds. Coordination Chemistry Reviews 249, 1641–1652.

Liu, Z.-P., Hu, P., 2002a. A density functional theory study on the active center of Fe-only hydrogenase: characterization and electronic structure of the redox states. Journal of the American Chemical Society 124, 5175–5182.

Liu, Z.-P., Hu, P., 2002b. Mechanism of H_2 metabolism on Fe-only hydrogenases. Journal of Chemical Physics 117, 8177–8180.

Löscher, S., Schwartz, L., Stein, M., Ott, S., Haumann, M., 2007. Facilitated hydride binding in an Fe–Fe hydrogenase active-site biomimic revealed by X-ray absorption spectroscopy and DFT calculations. Inorganic Chemistry 46, 11094–11105.

Lyon, E.J., Georgakaki, I.P., Reibenspies, J.H., Darensbourg, M.Y., 1999. Carbon monoxide and cyanide ligands in a classical organometallic complex model for Fe-only hydrogenase. Angewandte Chemie, International Edition 38, 3178–3180.

Morris, R.H., 2006. Hydrogenases and model complexes. In: Kraatz, H.-B., Metzler-Nolte, N. (Eds.), Concepts and Models in Bioinorganic Chemistry. Wiley-VCH, Weinheim, pp. 331–362.

Nicolet, Y., Piras, C., Legrand, P., Hatchikian, C.E., Fontecilla-Camps, J.C., 1999. Desulfovibrio desulfuricans iron hydrogenase: the structure shows unusual coordination to an active site Fe binuclear center. Structure 7, 13–23.

Pandey, A.S., Harris, T.V., Giles, L.J., Peters, J.W., Szilagyi, R.K., 2008. Dithiomethylether as a ligand in the hydrogenase H-cluster. Journal of the American Chemical Society 130, 4533–4540.

Penner-Hahn, J.E., 2005. Characterization of ''spectroscopically quiet'' metals in biology. Coordination Chemistry Reviews 249, 161–177.

Peters, J.W., Lanzilotta, W.N., Lemon, B.J., Seefeldt, L.C., 1998. X-ray crystal structure of the Fe-only hydrogenase (CpI) from Clostridium pasteurianum to 1.8 Å resolution. Science 282, 1853–1858.

Petrenko, T., Sturhahn, W., Neese, F., 2007. First-principles calculation of nuclear resonance vibrational spectra. Hyperfine Interactions 175, 165–174.

Razavet, M., Davies, S.C., Hughes, D.L., Pickett, C.J., 2001. {2Fe3S} clusters related to the di-iron sub-site of the H-centre of all-iron hydrogenases. Chemical Communications, 847–848.

Rubio, L.M., Ludden, P.W., 2008. Biosynthesis of the iron-molybdenum cofactor of nitrogenase. Annual Review of Microbiology 62, 93–111.

Schmidt, M., Contakes, S.M., Rauchfuss, T.B., 1999. First generation analogues of the binuclear site in the Fe-Only hydrogenases: $[Fe_2(m\text{-}SR)_2(CO)_4(CN)_2]^{2-}$. Journal of the American Chemical Society 121, 9736–9737.

Schunemann, V., Winkler, H., 2000. Structure and dynamics of biomolecules studied by Mossbauer spectroscopy. Reports on Progress in Physics 63, 263–353.

Shima, S., Pilak, O., Vogt, S., Schick, M., Stagni, M.S., Meyer-Klaucke, W., Warkentin, E., Thauer, R.K., Ermler, U., 2008. The crystal structure of [Fe]-hydrogenase reveals the geometry of the active site. Science 321, 572–575.

Siegbahn, P.E.M., Tye, J.W., Hall, M.B., 2007. Computational studies of [NiFe] and [FeFe] hydrogenases. Chemical Reviews 107, 4414–4435.

Smith, B.E., 2002. Structure: nitrogenase reveals its inner secrets. Science 297, 1654–1655.

Song, L.-C., Yang, Z.-Y., Bian, H.-Z., Hu, Q.-M., 2004. Novel single and double Diiron oxadithiolates as models for the active site of [Fe]-only hydrogenases. Organometallics 23, 3082–3084.

Spiro, T.G., 2007. Adventures in bioinorganic chemistry. Inorganic Chemistry 46, 10968–10980.

Strange, R.W., Eady, R.R., Lawson, D., Hasnain, S.S., 2003. XAFS studies of nitrogenase: the MoFe and VFe proteins and the use of crystallographic coordinates in three-dimensional EXAFS data analysis. Journal of Synchrotron Radiation 10, 71–75.

Sturhahn, W., 2004. Nuclear resonant spectroscopy. Journal of Physics: Condensed Matter 16, S497–S530.

Tard, C., Liu, X., Ibrahim Saad, K., Bruschi, M., De Gioia, L., Davies, S.C., Yang, X., Wang, L.-S., Sawers, G., Pickett, C.J., 2005. Synthesis of the H-cluster framework of iron-only hydrogenase. Nature 433, 610–613.

Tolman, W.B., 2006. Activation of Small Molecules: Organometallic and Bioinorganic Perspectives. Wiley-VCH, Weinheim.

Tye, J.W., Darensbourg, M.Y., Hall, M.B., 2006. Correlation between computed gas-phase and experimentally determined solution-phase infrared spectra: models of the iron-iron hydrogenase enzyme active site. Journal of Computational Chemistry 27, 1454–1462.

van der Vlugt, J.I., Rauchfuss, T.B., Whaley, C.M., Wilson, S.R., 2005. Characterization of a diferrous terminal hydride mechanistically relevant to the Fe-only hydrogenases. Journal of the American Chemical Society 127, 16012–16013.

Vignais, P.M., Billoud, B., 2007. Occurrence, classification, and biological function of hydrogenases: an overview. Chemical Reviews 107, 4206–4272.

Vincent, K.A., Parkin, A., Armstrong, F.A., 2007. Investigating and exploiting the electrocatalytic properties of hydrogenases. Chemical Reviews 107, 4366–4413.

Volbeda, A., Charon, M.-H., Piras, C., Hatchikian, E.C., Frey, M., Fontecilla-Camps, J.C., 1995. Crystal structure of the nickel-iron hydrogenase from Desulfovibrio gigas. Nature 373, 580–587.

Zampella, G., Greco, C., Fantucci, P., De Gioia, L., 2006. Proton reduction and dihydrogen oxidation on models of the $[2Fe]_H$ cluster of [Fe] hydrogenases. A density functional theory investigation. Inorganic Chemistry 45, 4109–4118.

Zhang, H.H., Hedman, B., Hodgson, K.O., 1999. X-ray absorption spectroscopy and EXAFS analysis: the multiple-scattering method and applications in inorganic and bioinorganic chemistry. In: Solomon, E.I., Lever, A.B.P. (Eds.), Inorganic Electronic Structure and Spectroscopy, Vol. 1. Wiley, New York, pp. 513–554.

Zhao, X., Georgakaki, I.P., Miller, M.L., Mejia-Rodriguez, R., Chiang, C.-Y., Darensbourg, M.Y., 2002. Catalysis of H_2/D_2 scrambling and other H/D exchange processes by [Fe]-hydrogenase model complexes. In: Inorganic Chemistry. Vol. 41, pp. 3917–3928.